C.P. No. 1198

MINISTRY OF DEFENCE (PROCUREMENT EXECUTIVE)

AERONAUTICAL RESEARCH COUNCIL

CURRENT PAPERS

Pressure Distributions at $M_\infty = 3.51$ and at High Incidences on Four Wings with Delta Planform

By

R. Hillier

Cambridge University Engineering Department

Communicated by Dr. L. C. Squire

LONDON. HER MAJESTY'S STATIONERY OFFICE

1972

Price 55p net

CP No. 1198
March 1971

Pressure Distributions at $M_\infty = 3.51$ and at High Incidences on Four Wings with Delta Planform

by R. Hillier

Cambridge University Engineering Department*

Communicated by Dr. L. C. Squire

Summary

Results are presented for wind tunnel tests at $M_\infty = 3.51$ on four wings with pointed vertices and sharp leading edges. Two conical models were tested through a wide range of angles of incidence and yaw and the results clearly demonstrate the stabilising effect of dihedral. Two simple non-conical wings were also tested and it is shown, in this case, that the pressure on the compression surfaces may be approximately deduced from an 'equivalent' conical wing.

---

* Now at Central Electricity Research Laboratories

** Replaces A.R.C.32 828

1. Introduction

In recent years there has been considerable interest in predicting the performance of lifting vehicles for flight at high supersonic and hypersonic speeds. During a programme to study the applications of thin shock layer theory* to wings for such vehicles the present author also undertook some pressure plotting experiments in the supersonic wind tunnels of the Cambridge University Engineering Department. Although the wind tunnel tests were designed to check specific theoretical points they provided results of sufficient interest to be worth presenting as a separate experimental report. The tests were conducted at a Mach number of 3.51** and basically comprised two parts. The first tested two conical wings (one with a flat compression surface and the other with a 'lens' type cross section) over a wide range of angles of incidence and yaw. There had been little previous work on yawed wings at these speeds, the most detailed being that of Larcombe[5] for a flat delta. Generally Larcombe's results were at a lower incidence range than that of this present report. Subsequent to the conical tests the flat delta was bent twice to provide some chordwise camber. Such a wing is an important shape from the viewpoint of thin shock layer theory and is termed the simply cambered wing (Ref. 4).

The bulk of the pressure plotting tests was made upon the compression surfaces although some limited suction surface measurements were also made. In all cases the shock was detached from the leading edges.

2. Experimental Details

2.1 Details of models

2.1a Conical models

Full details of the model designs are given in Figures 1a - 1c. Models 1 and 2 have delta planforms with leading edge sweep angles of 74.55° and 72.95° respectively. Model 1 has a flat compression surface whilst that of model 2 is a section of a right circular cone. For calculation purposes this latter section may be accurately represented by

$$\frac{\bar{y}}{\bar{x}} = 0.0852 \left(1 - 16.5 \frac{\bar{z}^2}{\bar{x}^2}\right)$$

where the coordinate system is based upon the plane of the leading edge as shown in Figure 1b.

The suction surfaces were given a minimum thickness, subject to requirements of strength and static tube accessibility, in order

---

* Thin shock layer theory has been discussed in a variety of papers and References 1 - 4 summarise most of the existing work as applied to wings.

** Thin shock layer theory effectively requires that the product of Mach number and incidence be large compared with unity; thus 'hypersonic' tests may be conducted at $M_\infty = 3.51$ provided that the incidence is high enough.

to reduce their interference upon the compression side. In both cases a triangular section was chosen to facilitate machining (see Figures 1a and 1b). Both models were machined from a solid block of K-9 steel alloy. Static holes were provided in model 1 by laying copper tubing, of 2.42 mm outside diameter and 1.62 mm inside diameter, into grooves machined in the model surface. Araldite was cemented over these tubes and then 0.23 mm diameter static holes were drilled through to the tubes. For model 2 the static holes were drilled directly through the metal surface to static tubes just under this surface. The average static hole depth was 0.70 mm. The spanwise distribution of static holes is shown in Figures 1a and 1b. A further set of holes was drilled along the centreline of model 1 for conical flow tests.

2.1.b Cambered models

The cambered wings (models 3 and 4) were made by bending model 1 in a carefully machined mould. After each bending the static tubes were completely relaid. Careful measurements across the span, on both models, detected no warping due to bending. Model 3 resulted in a form with constant radius of curvature and a change of incidence of 4.6° over the chord $\bar{c}$, i.e. the distance from the apex to the rearmost static hole position. The shape is very closely approximated by

$$\frac{\bar{y}}{\bar{c}} = -0.0402\left(\frac{\bar{x}}{\bar{c}}\right)^2$$

Model 4 was bent through 10.3° and resulted in a more complicated form which cannot accurately be represented by an equation of constant curvature (as could model 3) and higher terms in $\frac{\bar{x}}{\bar{c}}$ are required. Figure 1d shows the measured body ordinates along the centreline and also two analytic curves which have been fitted to them. The first is given by

$$\frac{\bar{y}}{\bar{c}} = -0.1350\left(\frac{\bar{x}}{\bar{c}}\right)^2 + 0.0295\left(\frac{\bar{x}}{\bar{c}}\right)^3$$

which matches the body slope at $\frac{\bar{x}}{\bar{c}} = 1.0$ and the ordinate $\bar{y}$ at $\frac{\bar{x}}{\bar{c}} = 0.75$. The second formulation adds a further term in $\left(\frac{\bar{x}}{\bar{c}}\right)^4$ to give

$$\frac{\bar{y}}{\bar{x}} = -0.1027\left(\frac{\bar{x}}{\bar{c}}\right)^2 - 0.0480\left(\frac{\bar{x}}{\bar{c}}\right)^3 + 0.0420\left(\frac{\bar{x}}{\bar{c}}\right)^4$$

where the body slope is now matched at $\frac{\bar{x}}{\bar{c}} = 1.0$ and the ordinate $\bar{y}$ at $\frac{\bar{x}}{\bar{c}} = 0.55$ and 1.0. When using the analytic representations for the body shape in theoretical calculations of the surface pressure there is not necessarily any advantage in adding extra terms in $\frac{\bar{x}}{\bar{c}}$, to the series above, since the prediction of body curvature and higher derivatives may in fact worsen. Another point

to note is that the planform shapes of models 3 and 4 are no longer strictly delta. However, the effect is small and only changes the effective sweep over the chord by about - 0.05° for model 3 and - 0.20° for model 4.

2.2 The wind tunnel and test conditions

All the tests were run in the Cambridge University Engineering Department supersonic wind tunnel at a nominal Mach number of 3.5. The tunnel is an intermittent blowdown tunnel, driven by compressed air, and has a working section area of 114 mm by 178 mm. A stagnation pressure of 7.58×10^5 N/m^2 gauge was used for all runs. The stagnation temperature varied slightly during a run giving a mean value of about 291°K with a variation of $\pm$ 4K°. Direct calibration of the tunnel showed a working section Mach number of 3.51 $\pm$ 0.02 with an upwash variation of $\pm$ 0.2°. The free stream Reynolds number, corresponding to the above conditions, was 49.8×10^6 per metre. Natural transition of the boundary layer was employed in all cases.

The model incidence was variable in the range - 5° to + 35° (see Figure 2 for nomenclature), the incidence being based upon the plane of the leading edges for the conical models and upon the plane of the leading edges at the vertex for the cambered wings. The general procedure was to start the tunnel with the model at zero incidence in order to reduce blockage effects. Once the supersonic flow was established the model was automatically moved to the required operating incidence. The angle of yaw was preset before each run by rolling the model about the sting support and then locking it in position. During tests, at any particular angle of yaw, measurements were taken in two runs using equal and opposite roll angles. This provided a better coverage of results for a given distribution of static holes and also enabled any three-dimensional disturbance to be partially smoothed out.

The incidence actually employed for measurements varied between about 12° and 30°. The upper limit was determined by a flow breakdown in which it became no longer possible to recover the flow behind the model with an oblique shock and a strong normal shock appeared. The subsequent separation of the tunnel wall boundary layer prohibited further tests. This breakdown occurred at 30° for model 1 and 28° for model 2.

All model pressures were recorded on a multi-tube mercury manometer.

2.3 Accuracy of the experiments

This can be effectively considered in two parts. Firstly there are the calibration errors. These comprise the major effect and arise from uncertainties in the incidence and yaw angles, coupled with the slight variation in flow conditions through the working section. The model incidence and yaw angles (relative to the tunnel datum) were repeatable, respectively, to $\pm$ 0.05° and $\pm$ 0.03°. When these are combined with the known variations in working section flowfield (see section 2.2) the calibration gives an accuracy of $\pm$ 0.25° in incidence, $\pm$ 0.03° in yaw and $\pm$ 0.02 in Mach number. Practically, this amounts to an error in

$\bar{p}/\bar{p}_{o\infty}$ of $\pm$ 0.11 x 10^{-2} at 12° incidence and $\pm$ 0.23 x 10^{-2} at 30°.

The second contribution to the errors results from the experimental techniques employed in recording the pressures, e.g. manometer errors, lags in pressure tubing and static hole imperfections. The manometers were read to an accuracy of $\pm$ 0.4 mm of mercury and since this also applies to the reference pressure there is a combined effect of $\pm$ 0.8 mm of mercury. The stagnation pressure was measured to within $\pm$ 0.125% by a Bourdon gauge on the settling chamber. Lags in the pressure tubing were negligible since ten seconds was sufficient for the readings to settle and a full run time of forty seconds was always employed. The influence of static hole imperfections is difficult to assess and results mainly from burrs, local deformations of the surface and the hole size. These all presumably contribute to the slight scatter observed in the pressure distributions although this is in fact explicable in terms of the calibration errors already discussed. A few tests were conducted with 0.76 mm holes in model 1. These pressures were the same as for the smaller holes, to within $\pm$ 0.025 x 10^{-2} in $\bar{p}/\bar{p}_{o\infty}$, nor was this systematic, so that hole size is unimportant. A final test to measure model bending under load showed no observable deflection.

The total experimental scatter expected from this second class of errors amounts to less than $\pm$ 0.040 x 10^{-2} in $\bar{p}/\bar{p}_{o\infty}$.

3. Presentation and Discussion of the Results

3.1 Conical flow tests

In a uniform incident flow, and in the absence of viscous and heat conduction effects, the flow over models 1 and 2 should be conical. Any experimental deviation from this, which is not accountable to the other errors already discussed, is a measure of the viscous interaction. The main mechanism of this interaction is in the boundary layer displacement of the outer flow and shock (from their inviscid values) which, in turn, raises the surface pressures. In the present experiments the Mach number was low and the Reynolds number high, both conditions which result in a weak interaction. This was in fact confirmed experimentally. Figure 3 shows the pressure distribution along the centreline of model 1 and the maximum deviation from a constant value is $\pm$ 0.15 x 10^{-2} in $\frac{\bar{p}}{\bar{p}_{o\infty}}$ with agreement much better generally. This is well within the maximum errors expected from the discussion of section 2.3 so that viscous interaction is unimportant in these tests.

3.2 Upper surface pressures

In any theoretical analysis of hypersonic wings it is generally assumed that the compression surface is independent of the suction side, even if the shock is detached from the leading edges. This requires very low suction surface pressures so that a supersonic expansion may set up about the leading edges. In practice, disturbances may manifest themselves via the boundary layer so that testing of any particular compression surface only

provides meaningful results when the extent of this interference has been assessed. Disturbances will be small for low suction surface pressures but, ideally, the best check would be to test the same compression surface with a variety of suction surface shapes. This was done, for example, by Squire[6] and Peckham[7]. They both deduced that the suction side had very little effect upon the compression surface for conditions closely related to the present work.

Limited suction surface pressures were recorded on model 1 at 90% span and 86.9 mm chord and on model 2 at 70% span and 85.2 mm chord. These are shown in Figure 4. Both curves exhibit a fall in pressure, for incidence increasing to 20°, at which position they rise again. This recompression is slight for model 1 but is very marked for model 2. The cause is uncertain but there are various possible mechanisms. Firstly, the trailing edge shock on the suction surface may separate the boundary layer for some distance forward of this position and thus influence the static pressure readings. This is unlikely, however, since schlieren visualisation during such runs (using a light beam normal to the working section) showed no such disturbance. A second, more likely, possibility is the occurrence of an embedded shock lying in a conical surface, or nearly so, so that it would not be visible in the schlieren. The sudden pressure rise with incidence would then mark the movement of such a shock, or a region of shock separated flow, as it passes over the static hole. There is a further possibility that the pressure variations indicate a change in the behaviour of a separated vortex type flow over the suction surface. Again, this would not be visible in the schlieren. The important point is whether this disturbance affects the compression surface and Figure 6a shows the corresponding spanwise pressure distributions on the compression surface of model 2. There are no sudden disturbances in the pressure as the incidence increases, even about 20°, so that it seems unlikely that there is a significant interference.

3.3 Spanwise pressure distributions on models 1 and 2

Figures 5a and 6a show the unyawed distributions across the span of models 1 and 2 respectively. Figure 5a exhibits the flatter distribution usually associated with flat deltas indicating that the shock, which is the main contributor to the pressure, is also very flat. The pressure distributions on model 2 are less constant, changing from a positive (outwards) gradient at low incidences to a quite strong negative gradient at the higher values. A similar distribution was also observed by Squire[8] in some tests on 'lens' section deltas. Since model 2 displaces the shock further from the plane of the leading edges, at any given incidence, the centreline pressure is higher on model 2 than on model 1.

Figures 5b - 5e and 6b - 6d are the spanwise pressure distributions across the two wings when yawed. The two sets of symbols indicate measurements taken with the equal and opposite roll angles. The small scatter between the two sets is a measure both of the accuracy with which the roll angle may be reproduced and also the weakness of any three-dimensional disturbances in the incident flow. The most important feature of these results is that the rolling moment is negative for positive roll, i.e. a stabilising moment. This rolling moment is clearly stronger for

model 2. Both these results were predicted by the thin shock layer theory[3,4] and demonstrate the inherent stabilising effect of wing thickness (or dihedral). The centreline pressure remains virtually constant as the wings yaw at constant incidence. This shows the insensitivity of the centreline shock position to yaw.

3.4 Cambered wing pressure distributions

Figures 7a and 7b show pressure distributions along the centrelines of models 3 and 4 respectively. The chordwise positions are normalised with respect to $\bar{c}$ the distance from the apex to the rearmost static hole position. The point at the vertex of each wing represents an interpolation from the results of model 1. Since the highest incidence tests were not covered by model 1 these points may be in some error. The variation of pressure along model 3 is almost perfectly linear within the experimental errors involved. It should be noted that this is a wing of constant curvature. For both models there is a considerable expansion along the centreline, halving the pressure level for model 4, which is in agreement with simple Prandtl-Meyer considerations. The centreline pressure along model 4 is also closely given by that on the 'equivalent' flat delta, i.e. the local pressure on the cambered wing is assumed to be given by the flat delta, of same sweep angle, flying at that local body incidence. Figure 8 is a typical comparison, using model 1 as the 'equivalent' delta, and tends to overpredict the pressure levels slightly; this is to be expected since, although it makes an accurate estimate of local shock pressure (due to body incidence) it makes no allowance for centrifugal or curvature effects. This technique may also prove useful for other simple, non-conical wings but cannot be applied with such ease to wings with complex planform shape and thickness distribution since the 'equivalent' delta is then by no means obsious.

Figures 7c and 7d show the unyawed spanwise distributions on models 3 and 4 at chordwise positions of 90.5 mm and 90.0 mm respectively, i.e. at $\bar{x}/\bar{c} = 1.0$ in both cases. As expected, these distributions are flat, hardly varying their form with incidence, although there is a slightly more marked tendency for a greater rise across the span at lower angles of incidence.

No detailed distributions were recorded on the cambered wings when yawed. However, a typical comparison between thin shock layer theory and experiment is shown in Figure 9 for two tests with model 4 yawed.

4. Concluding Remarks

The main conclusions of this work are that

i) for a large range of angles of incidence and yaw the conical models showed a stabilising rolling moment. This moment is greatest for the thickest wing and indicates the inherent stabilising effect of dihedral.

ii) the results are believed to indicate the behaviour of the particular compression surfaces tested and to be substantially independent of suction surface and viscous effects.

iii) the pressures on the simply cambered wing are closely predicted by the 'equivalent flat delta'.

Acknowledgements

During this research the author was financed by the Science Research Council. He would also like to express his gratitude to Dr. L.C. Squire of the Cambridge University Engineering Department who supervised the work.

List of Symbols

α	angle of incidence; defined as the incidence of the plane of the leading edges at the apex of the wing
β	angle of yaw
η	spanwise position
$\bar{c}$	chord
M_∞	free stream Mach number
$\bar{p}$	static pressure
$\bar{p}_{0\infty}$	free stream stagnation pressure
$\bar{x}$, $\bar{y}$, $\bar{z}$	Cartesian coordinates

List of References

1. L.C. Squire — Calculated pressure distributions and shock shapes on thick conical wings at high supersonic speeds. Aero. Quart. Vol. XVIII, pp.185-206, 1967.

2. P.L. Roe — Aerodynamic problems of hypersonic aircraft. Von Karman Institute short course, January 1970.

3. R. Hillier — The effects of yaw on conical wings at high supersonic speeds. Aero. Quart. Vol. XXI, pp.199-210, 1970.

4. R. Hillier — Some applications of thin shock layer theory to hypersonic wings. Ph.D. Dissertation, University of Cambridge, 1970.

5. M.J. Larcombe — An investigation of the flow around a delta wing with a triangular cross-section at a Mach number of 4.0. (Unpublished).

6. L.C. Squire — Pressure distributions and flow patterns at M = 4.0 on some delta wings. Part 1: Wings of inverted 'V' cross-section. Part II: 'Flat' wings. ARC R & M 3373, 1963.

7. D.H. Peckham — Pressure distribution measurements on a series of slender delta body shapes at Mach numbers of 6.85 and 8.60. ARC CP 791, 1964.

8. L.C. Squire — Pressure distributions and flow patterns on some conical shapes with sharp leading edges and symmetrical cross-sections at M = 4.0. ARC R & M 3340, 1962.

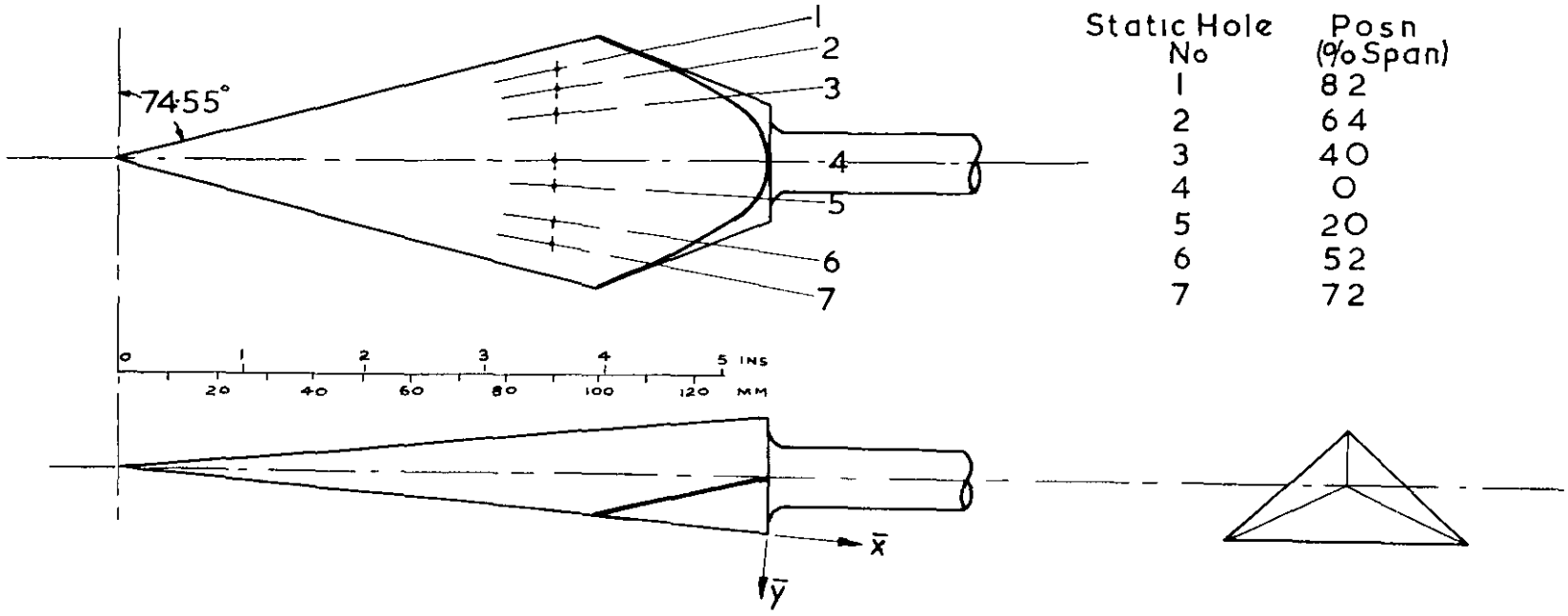

Static Hole No	Posn (% Span)
1	82
2	64
3	40
4	0
5	20
6	52
7	72

Figure 1a Design of Model 1

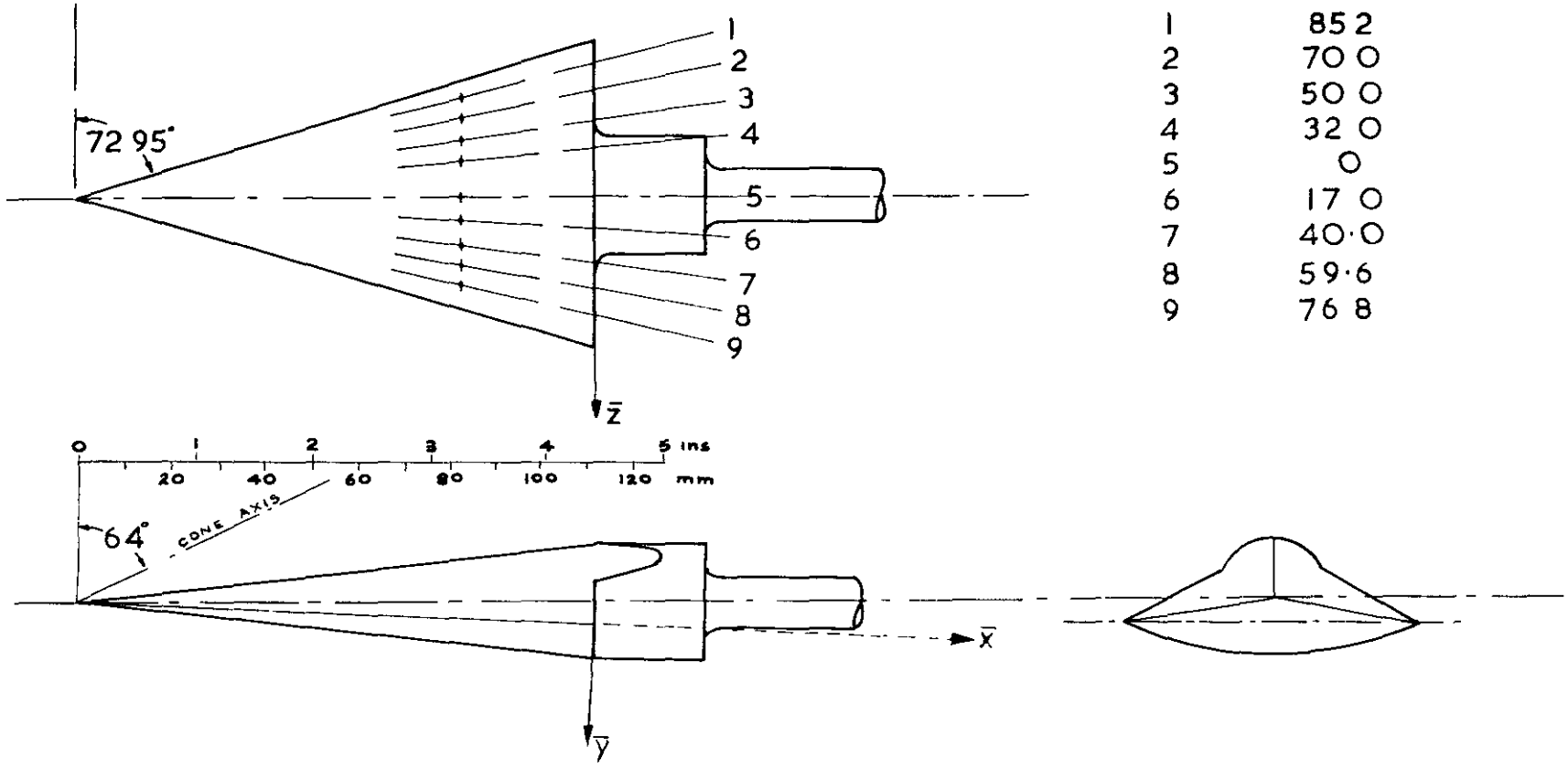

Static Hole No	Posn (% Span)
1	85 2
2	70 0
3	50 0
4	32 0
5	0
6	17 0
7	40·0
8	59·6
9	76 8

328 28

Figure 1b Design of Model 2

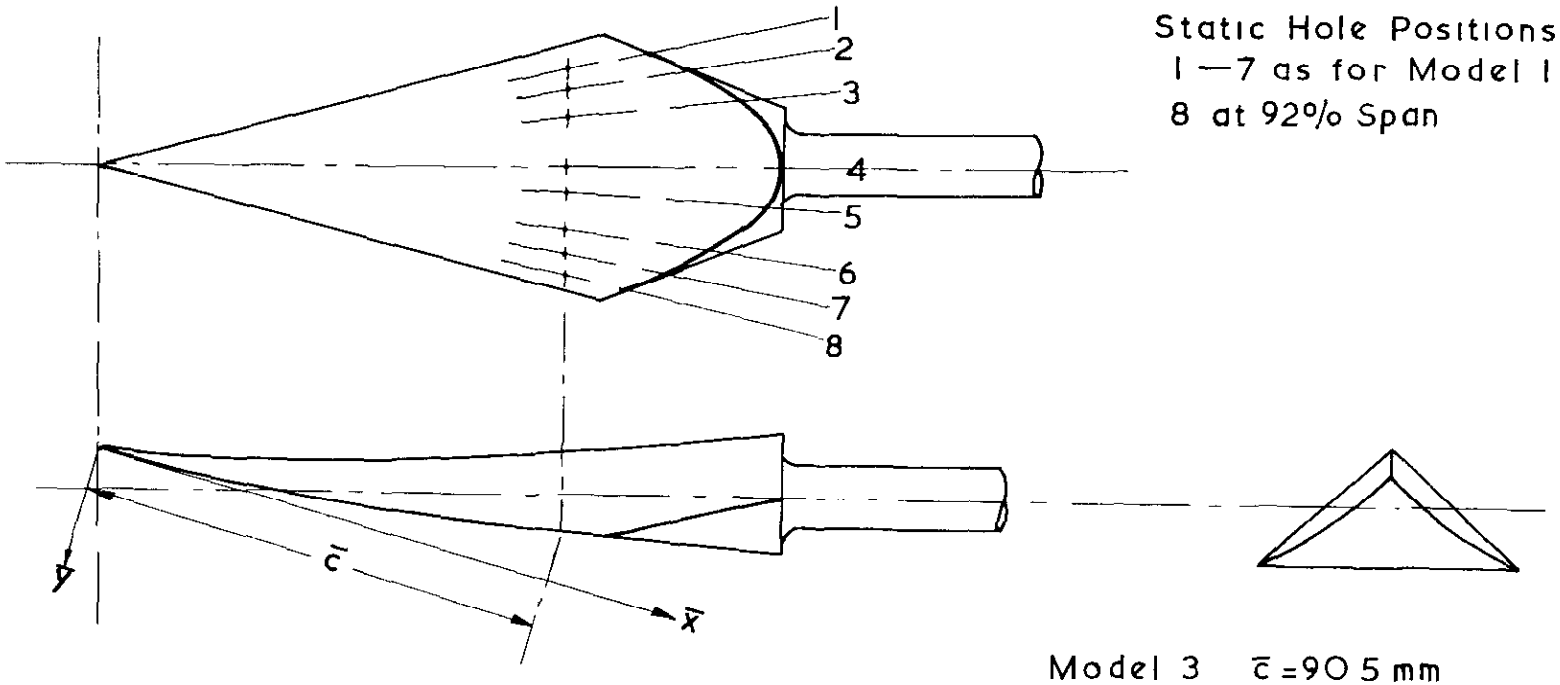

Static Hole Positions
1 — 7 as for Model 1
8 at 92% Span

Model 3 $\bar{c}$ = 90 5 mm
Model 4 $\bar{c}$ = 90 0 mm

Figure 1c Design of Models 3 & 4

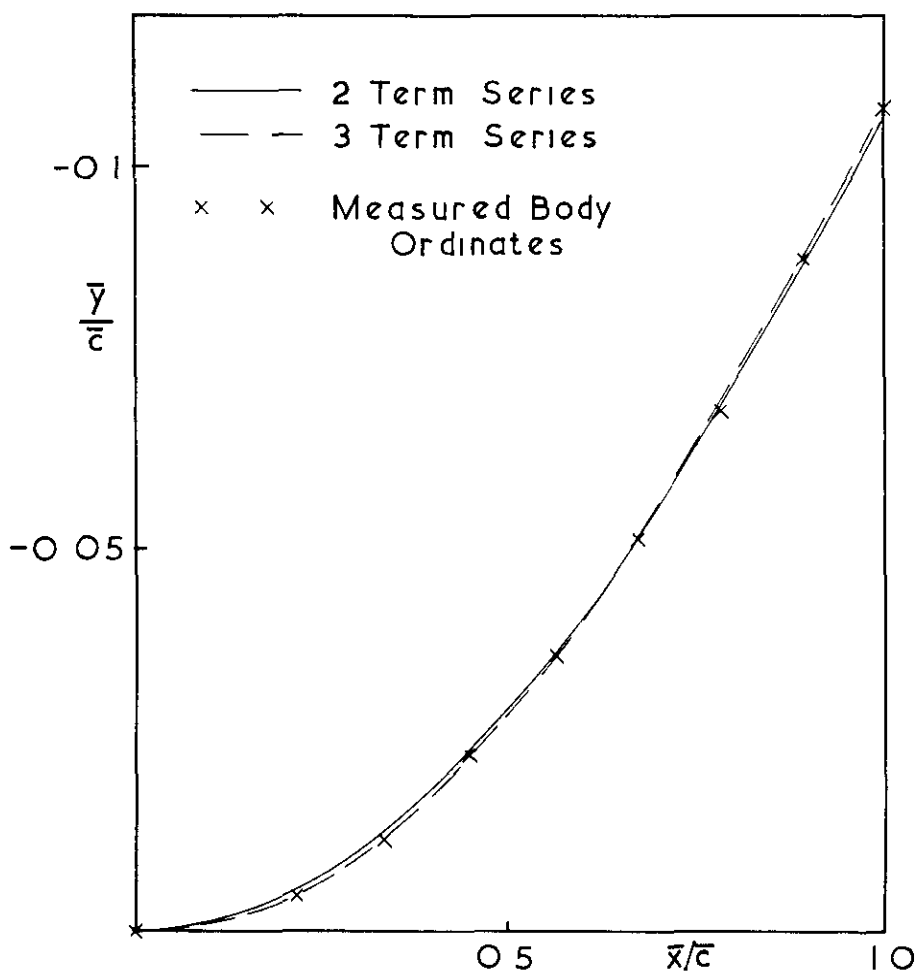

Figure Id Comparison between Measured Ordinates and Power Series for Model 4

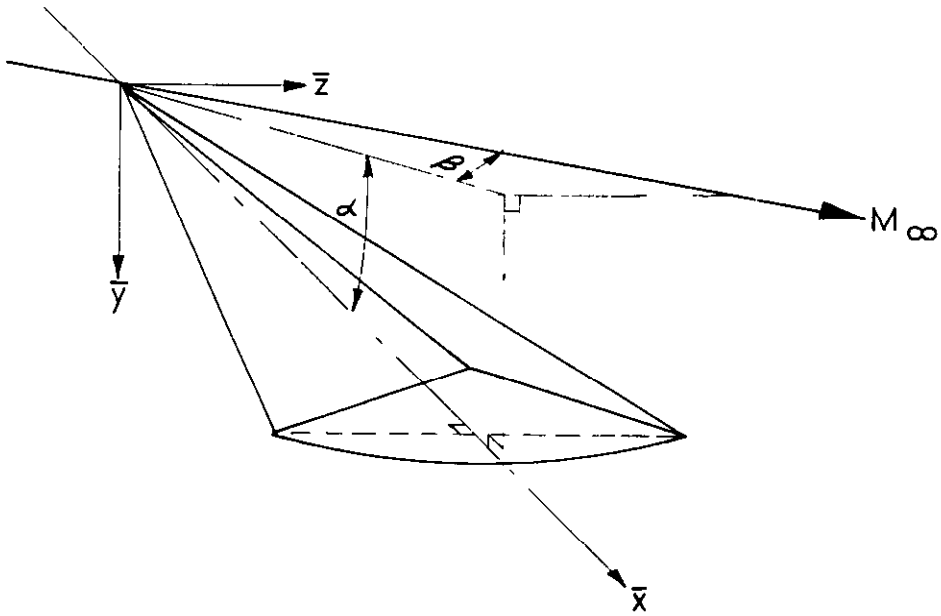

Typical Conical Wing

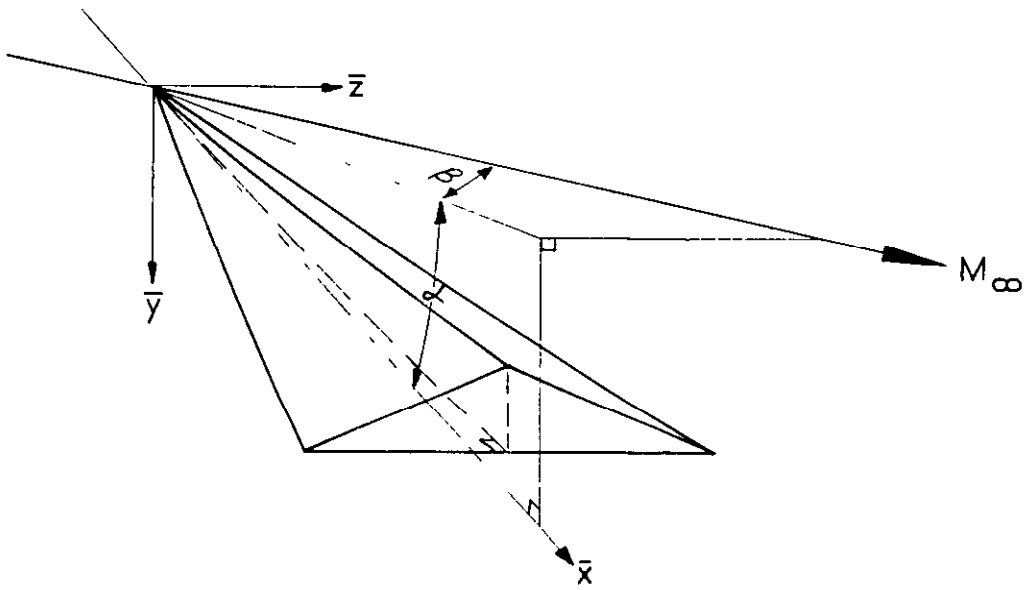

Simply Cambered Wing

Figure2 Nomenclature for the Yawed Wing

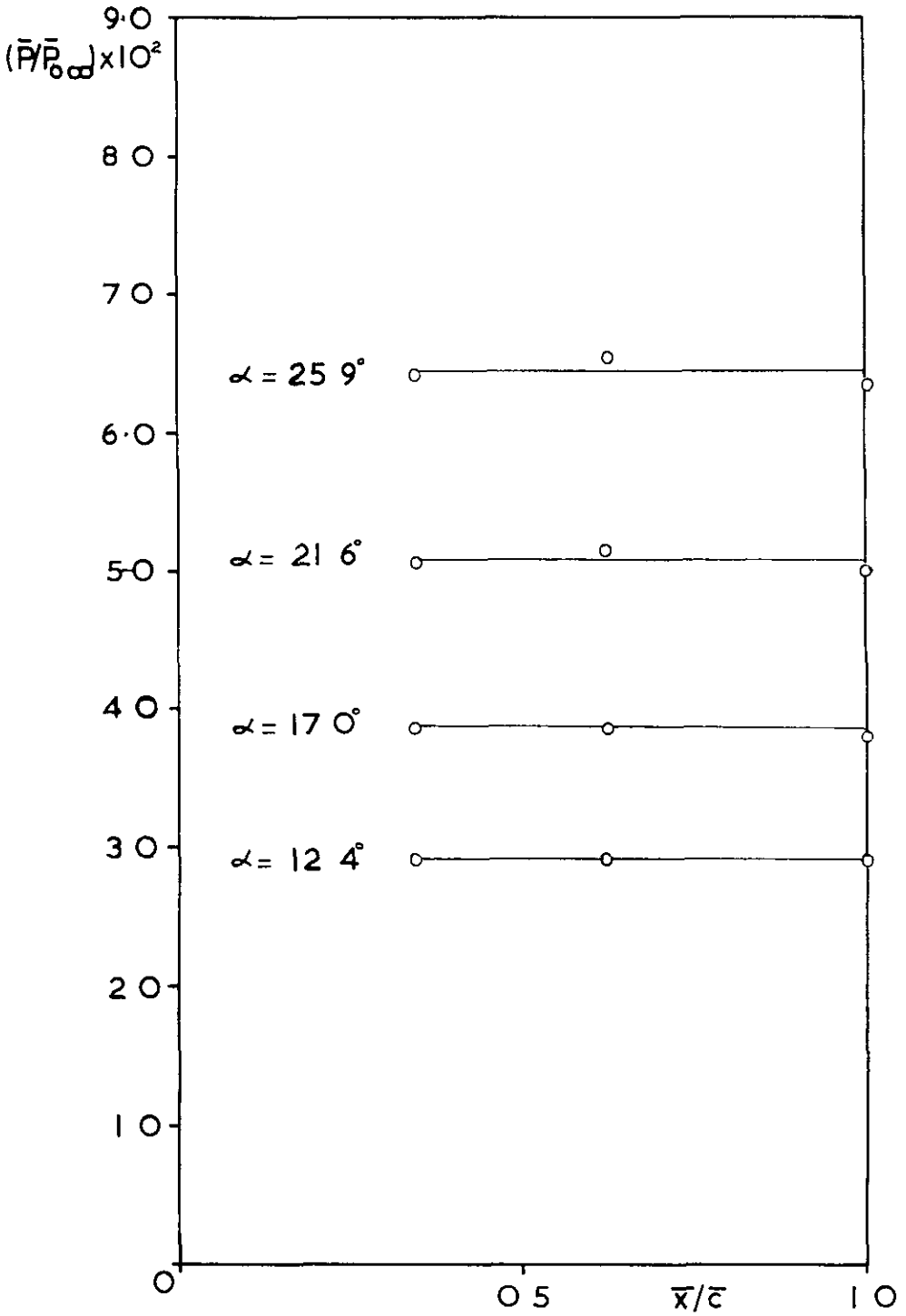

Figure 3 Pressure Distributions along Centreline of Model 1

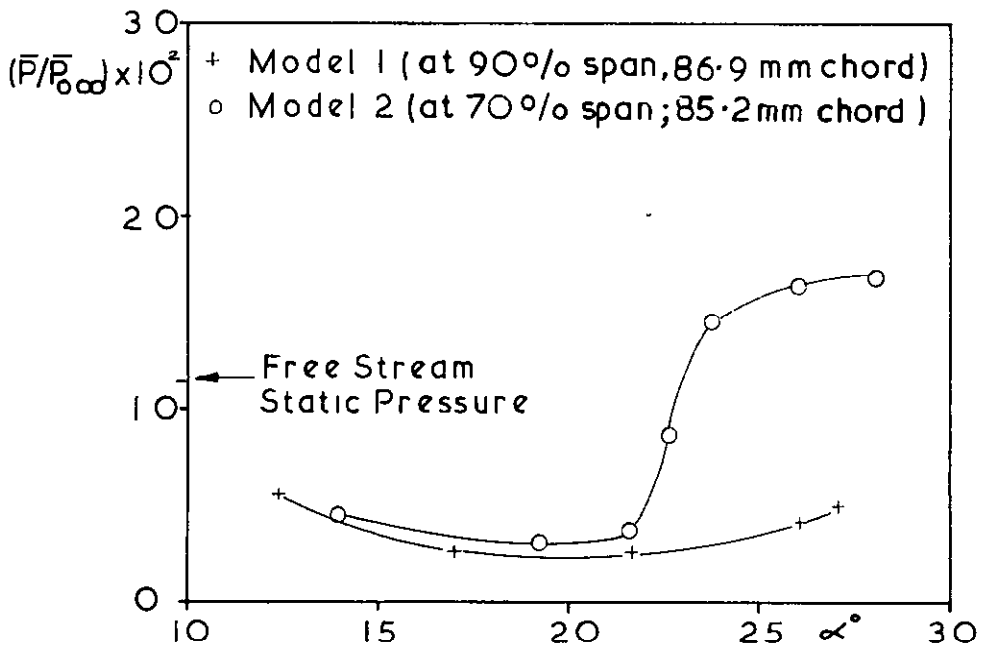

Figure 4 Pressures on Suction Surfaces of Models 1 & 2

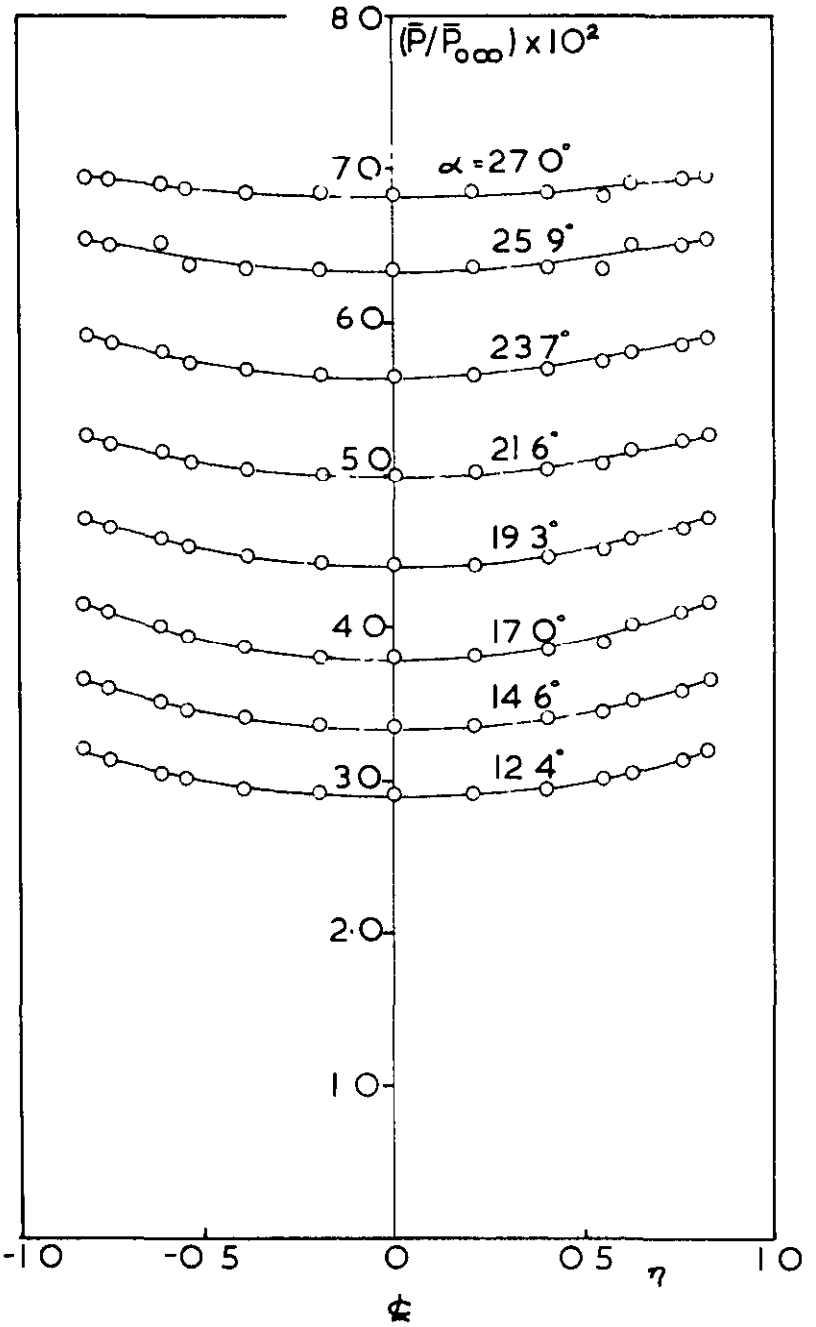

Figure 5a Spanwise Pressure Distributions on Model I

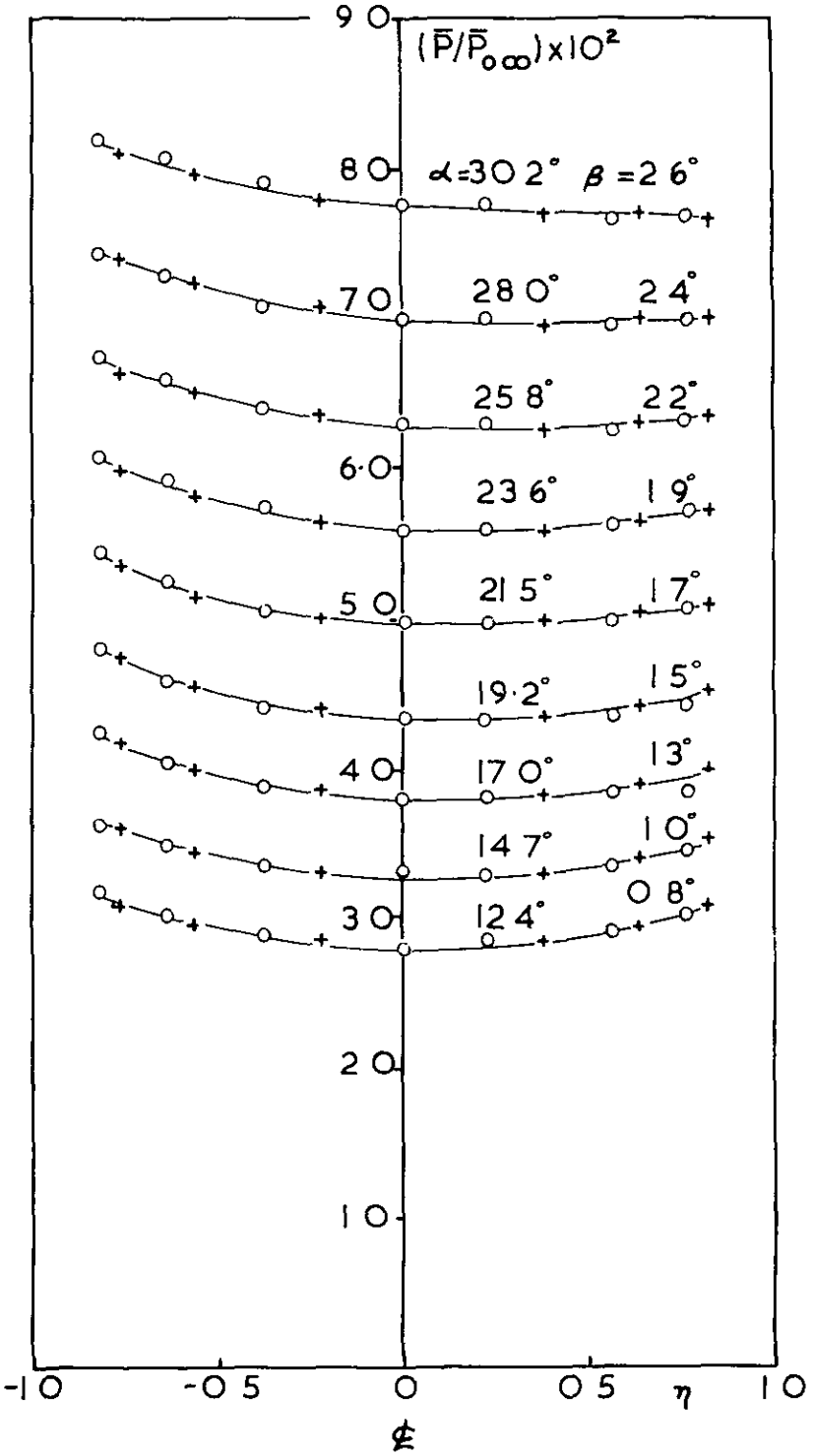

Figure 5b Spanwise Pressure Distributions on Model I

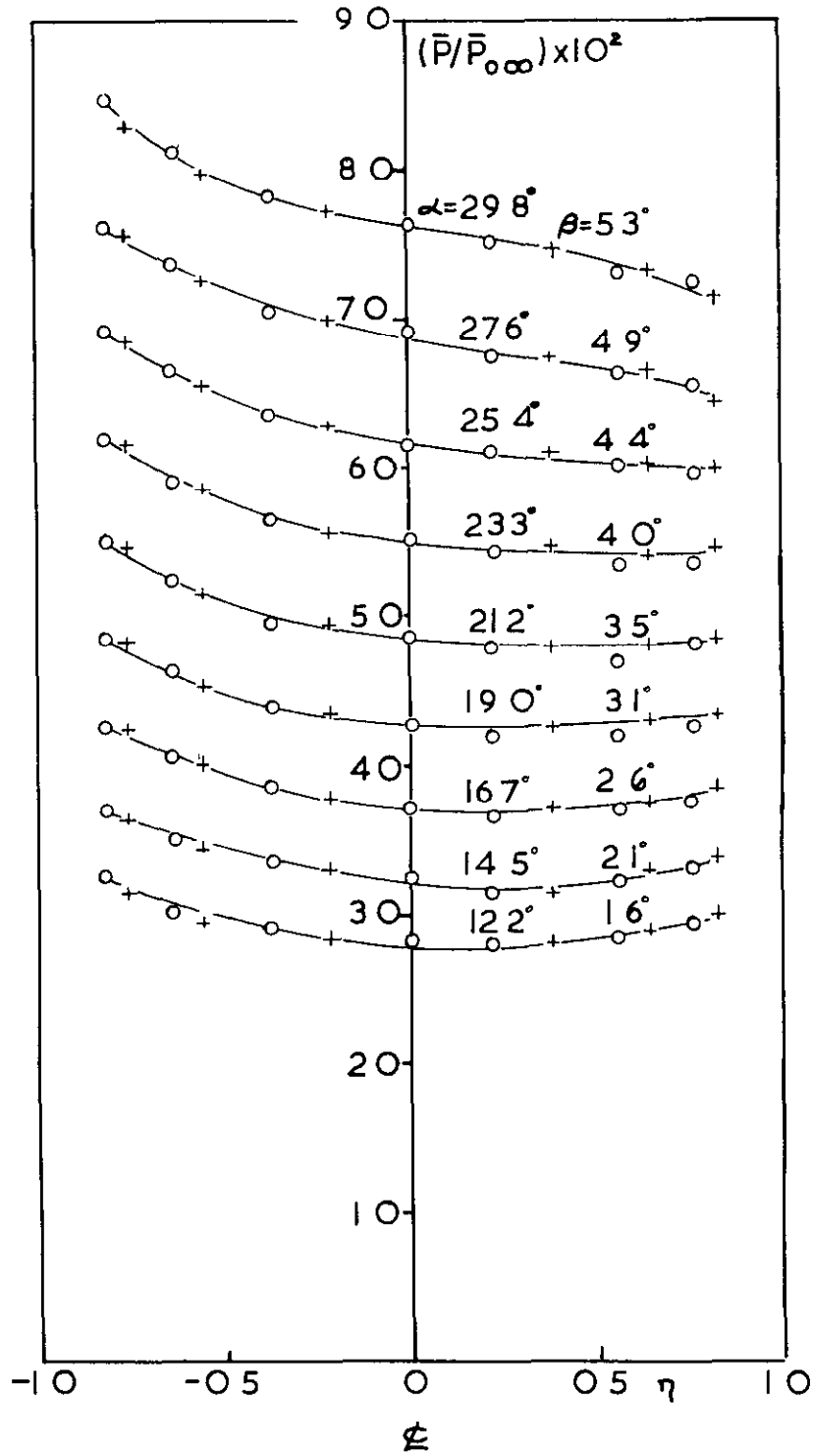

Figure 5c Spanwise Pressure Distributions on Model 1

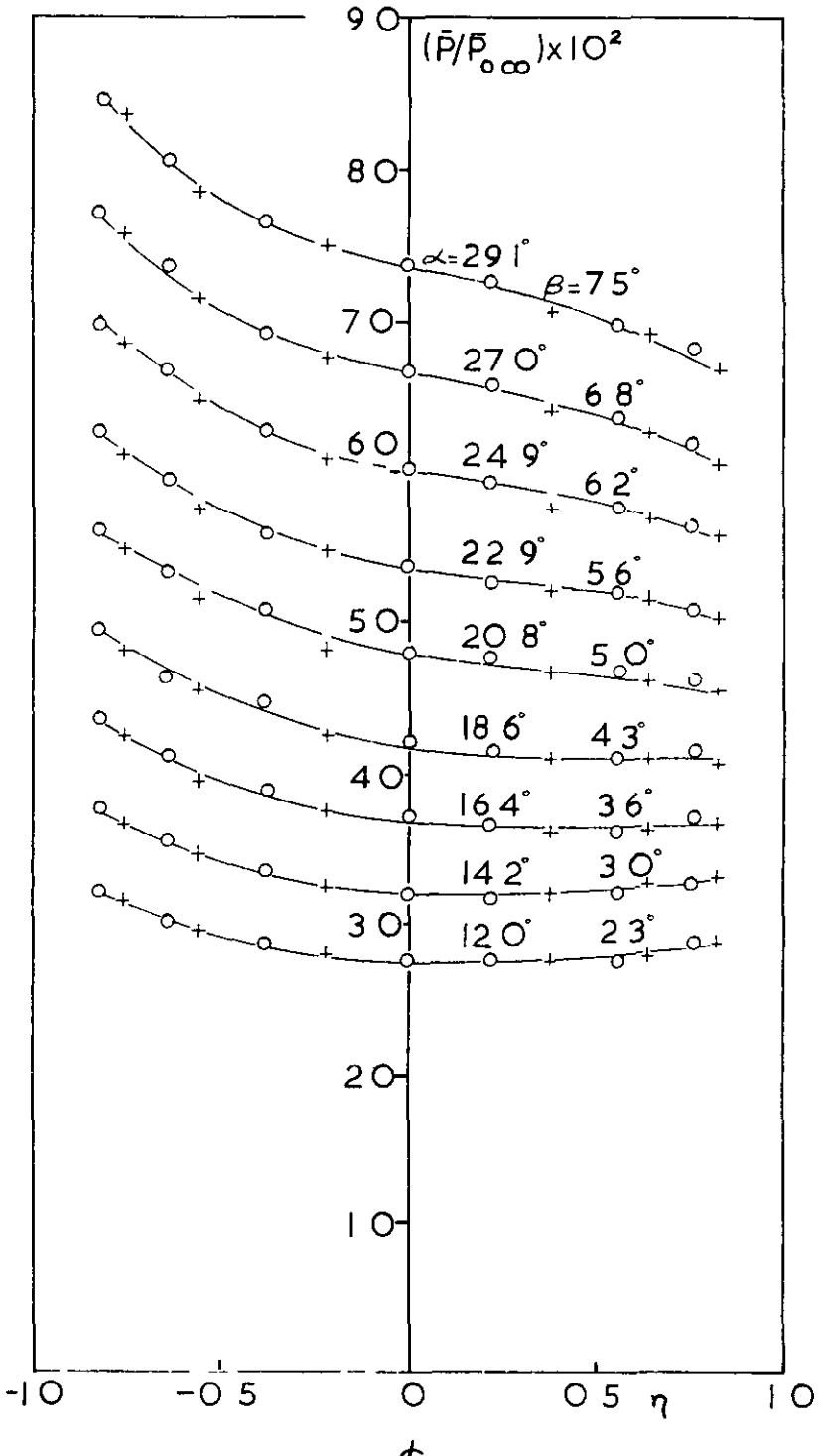

Figure 5d Spanwise Pressure Distributions on Model I

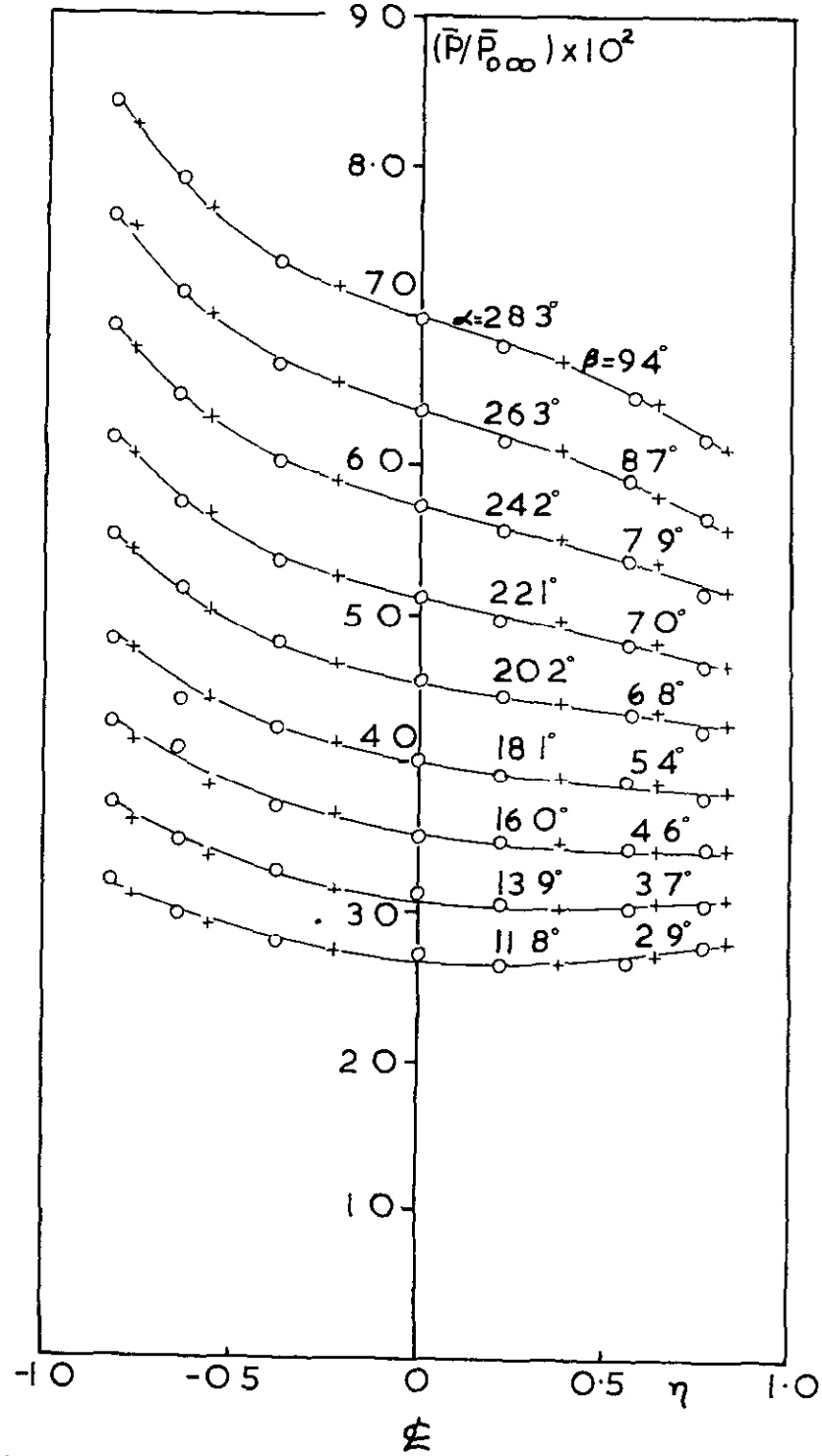

Figure 5e Spanwise Pressure Distributions on Model 1

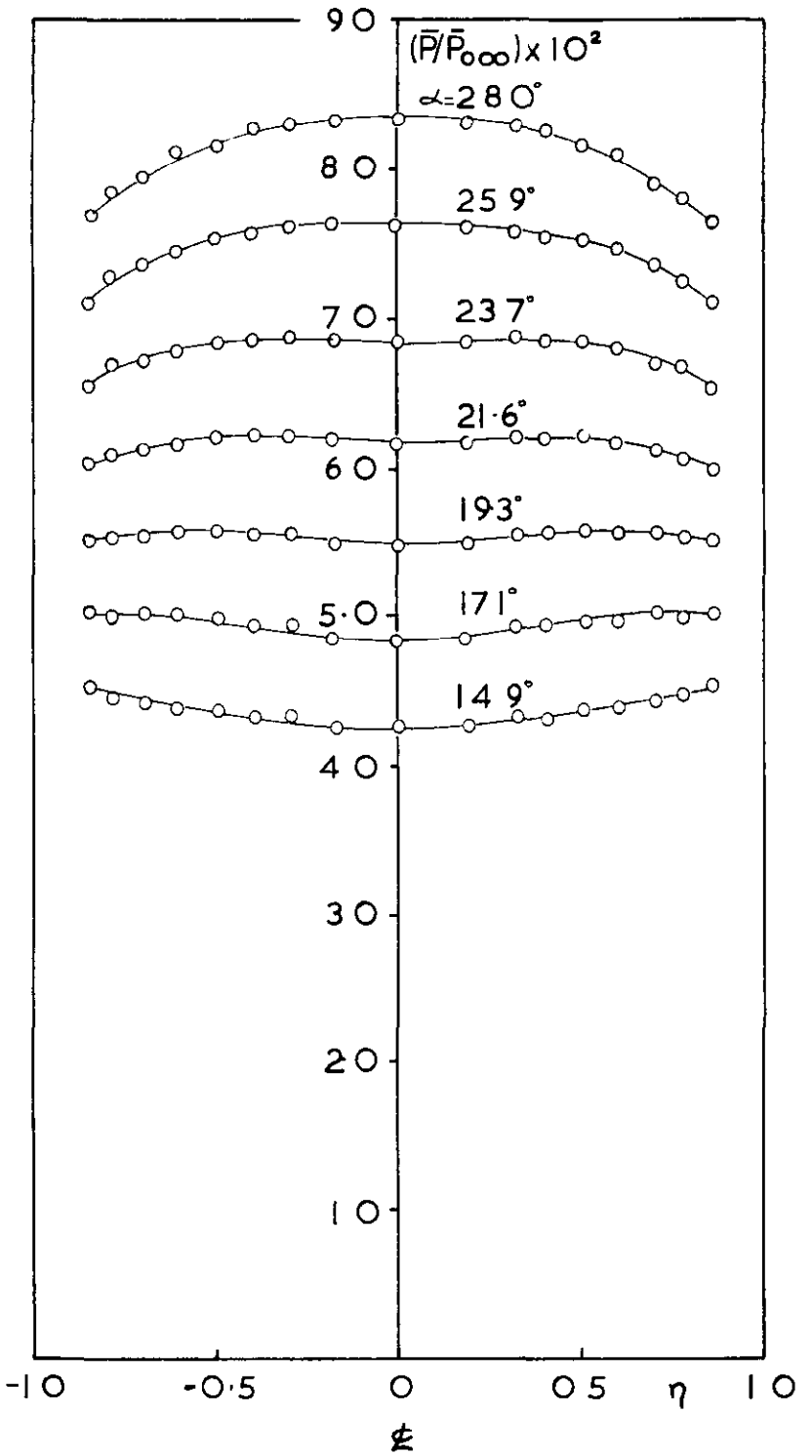

Figure 6a Spanwise Pressure Distributions on Model 2

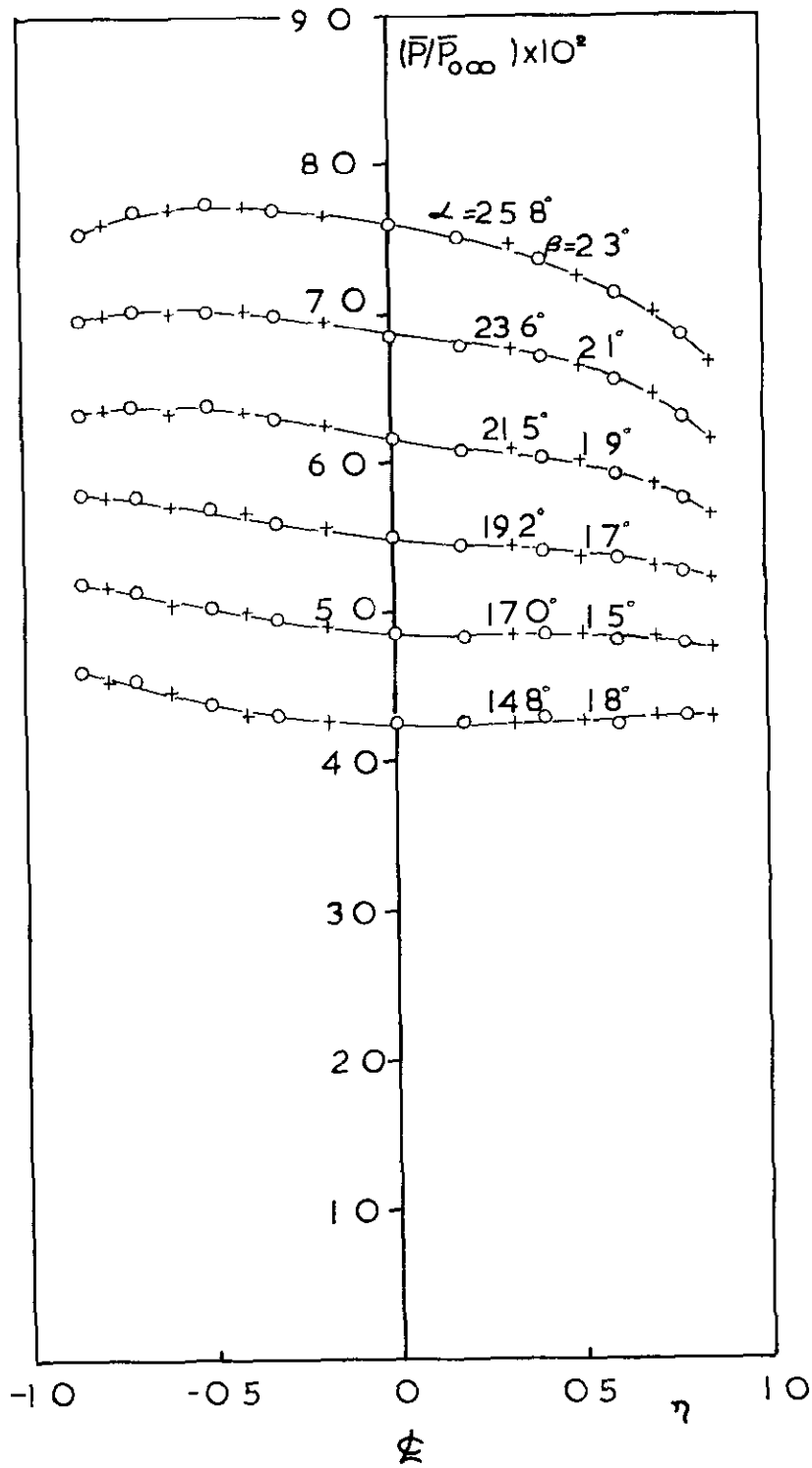

Figure 6b Spanwise Pressure Distributions on Model 2

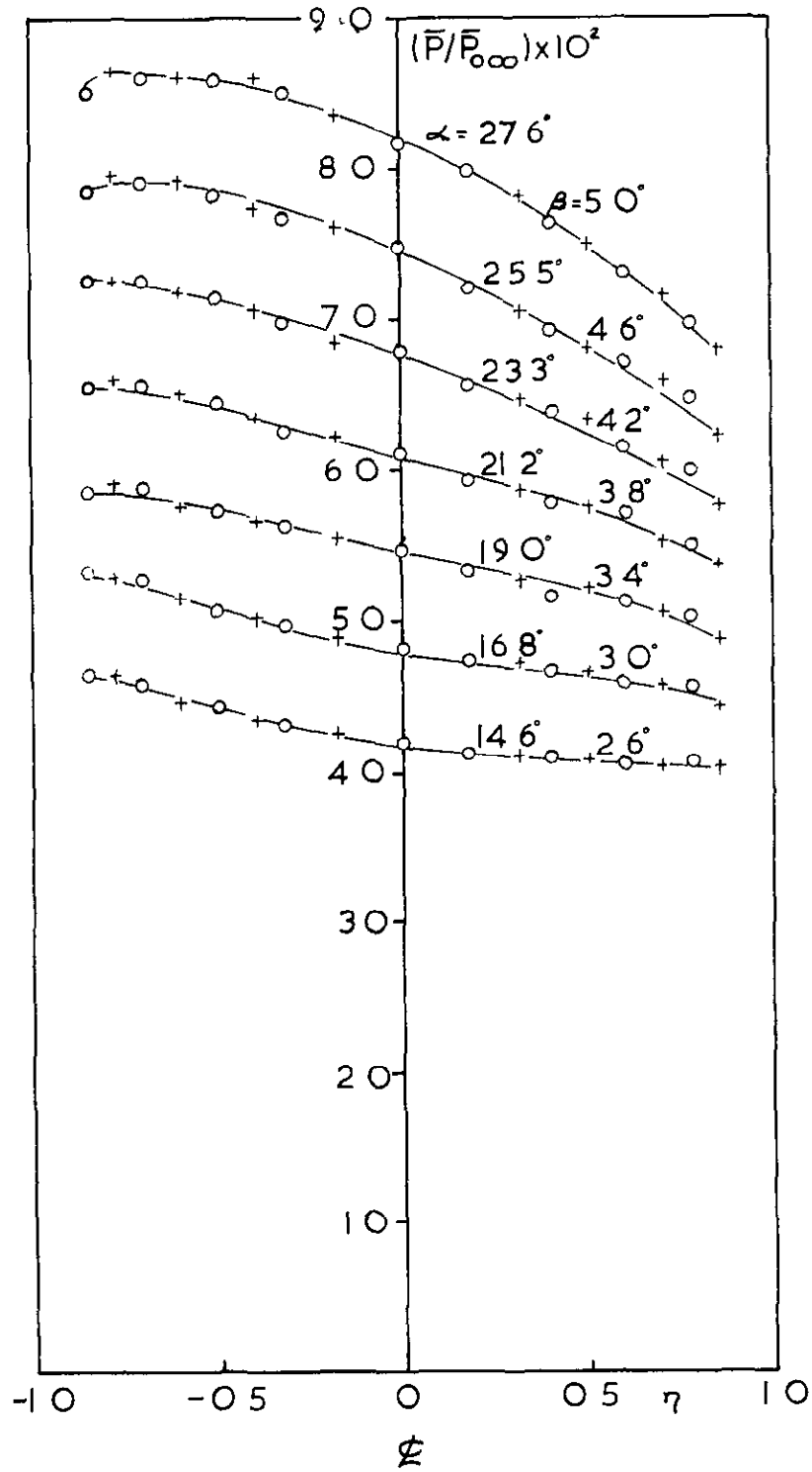

Figure 6c Spanwise Pressure Distributions on Model 2

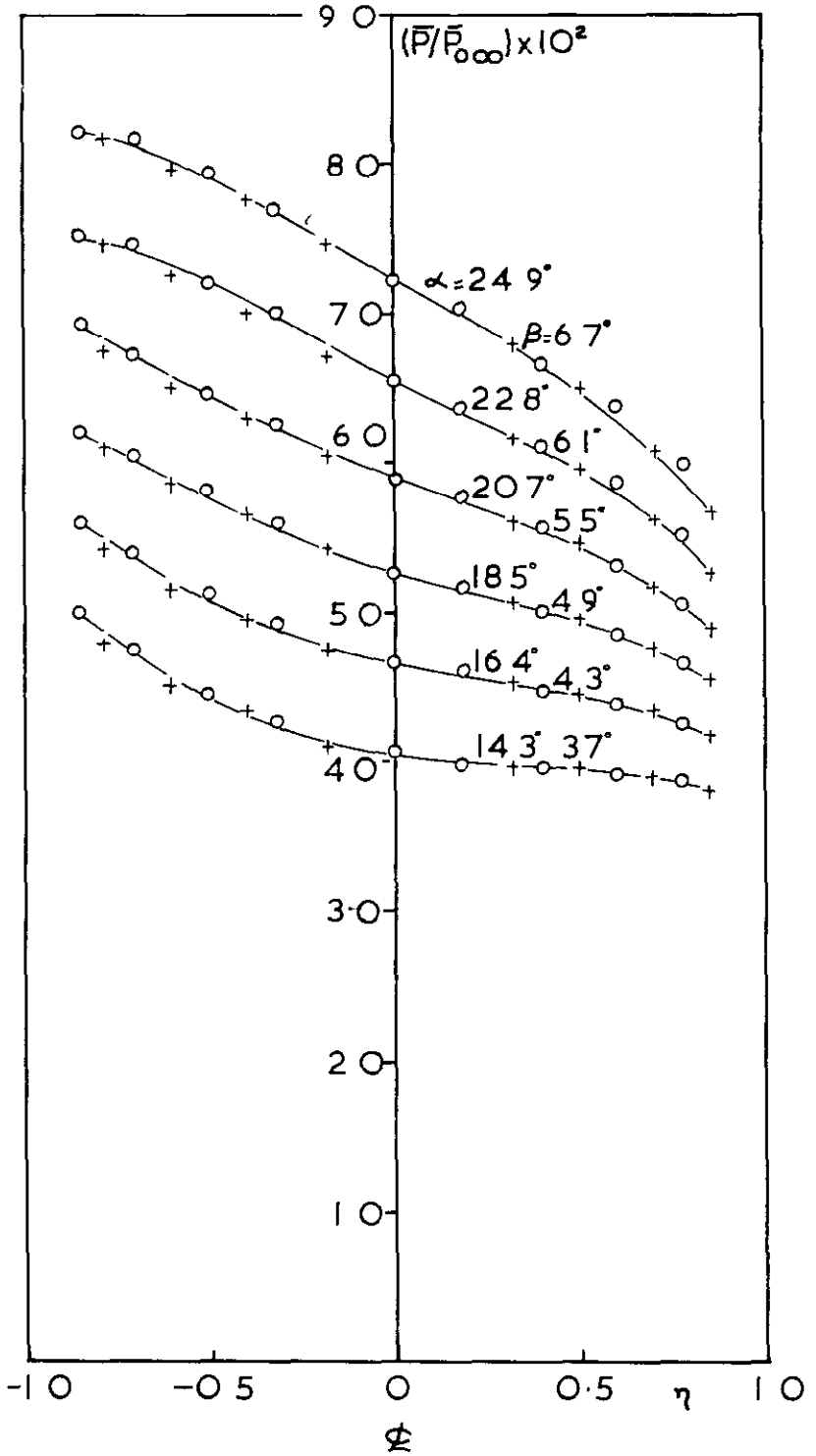

Figure 6d Spanwise Pressure Distributions on Model 2

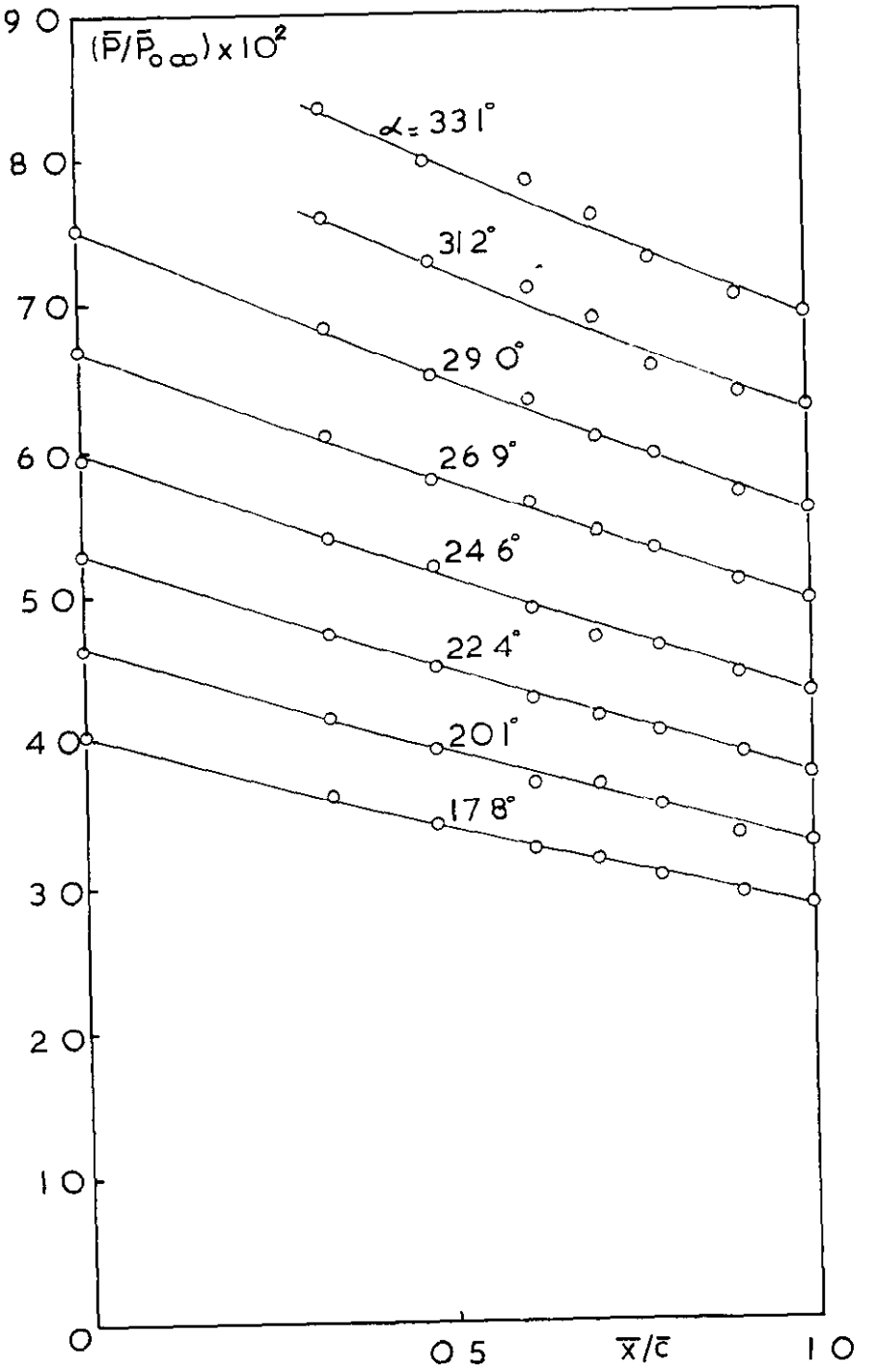

Figure 7a Pressure Distributions along Centreline of Model 3

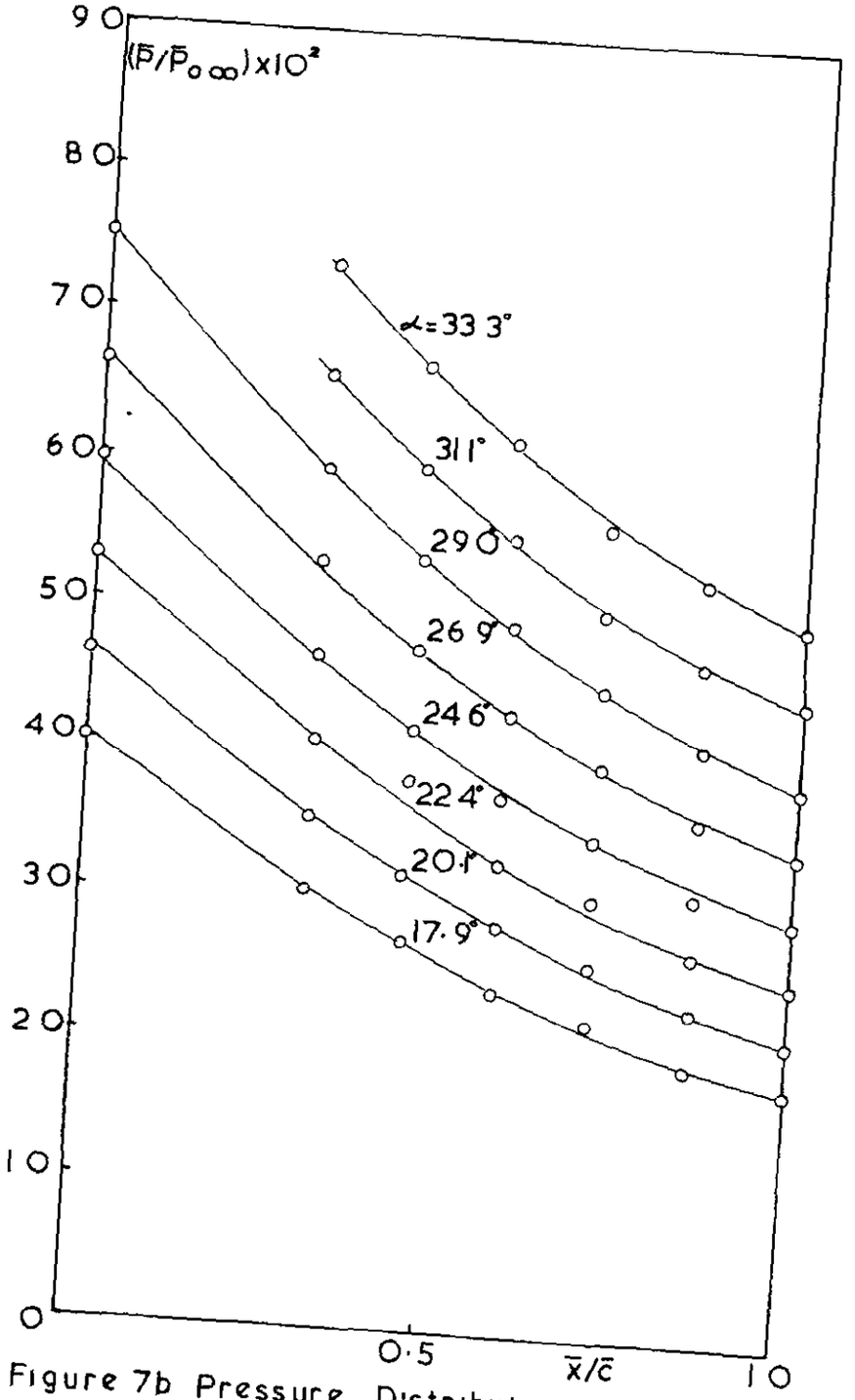

Figure 7b Pressure Distributions along Centreline of Model 4

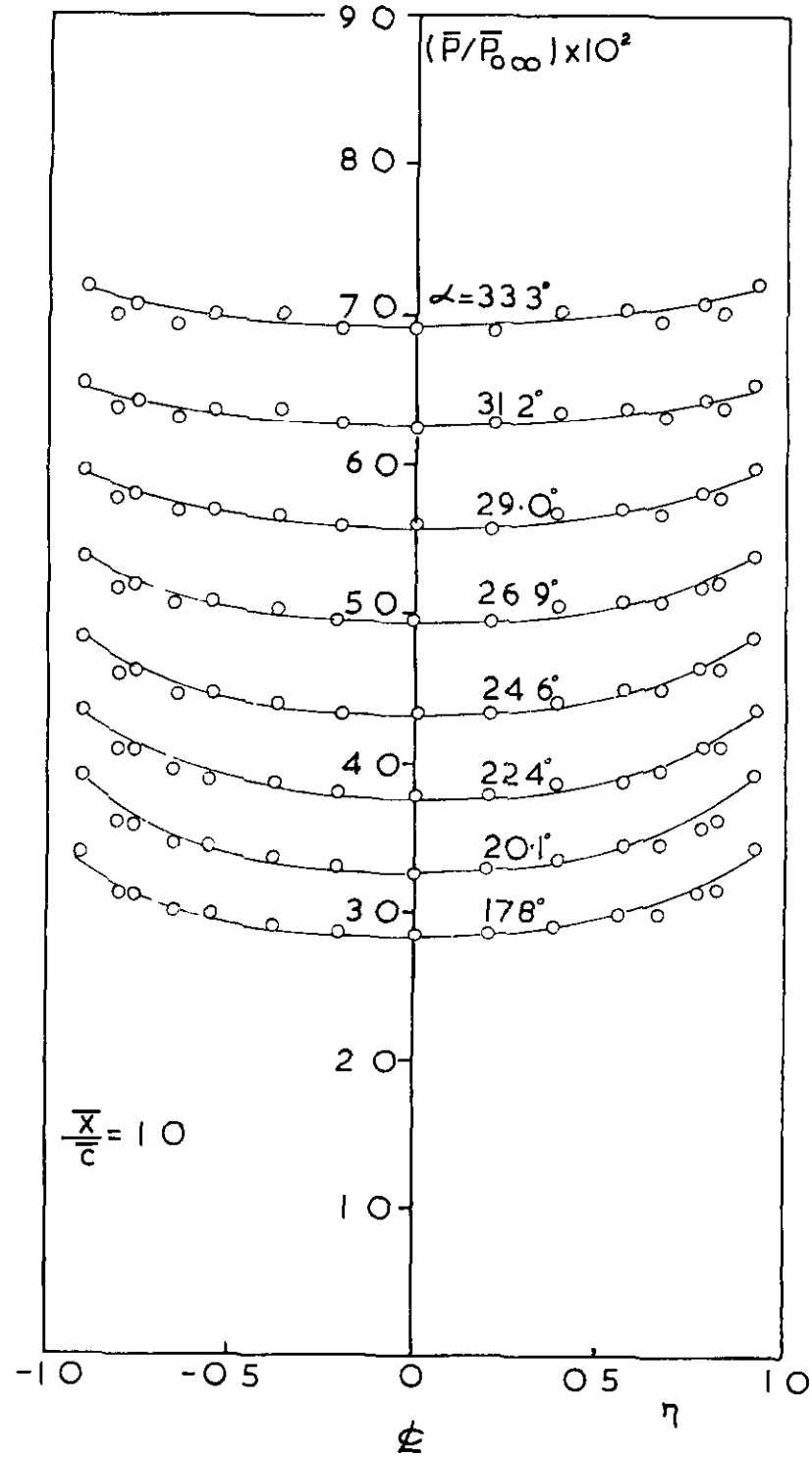

Figure 7c Spanwise Pressure Distributions on Model 3

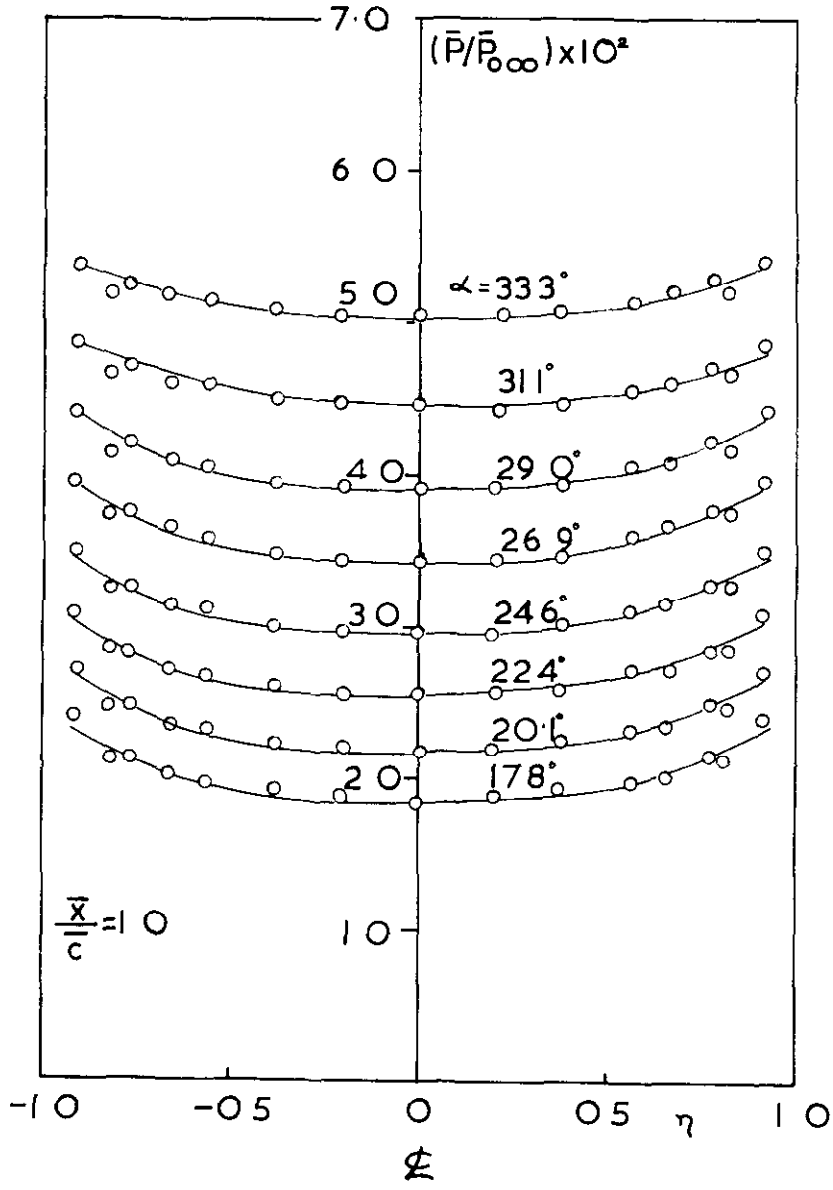

Figure 7d Spanwise Pressure Distributions on Model 4

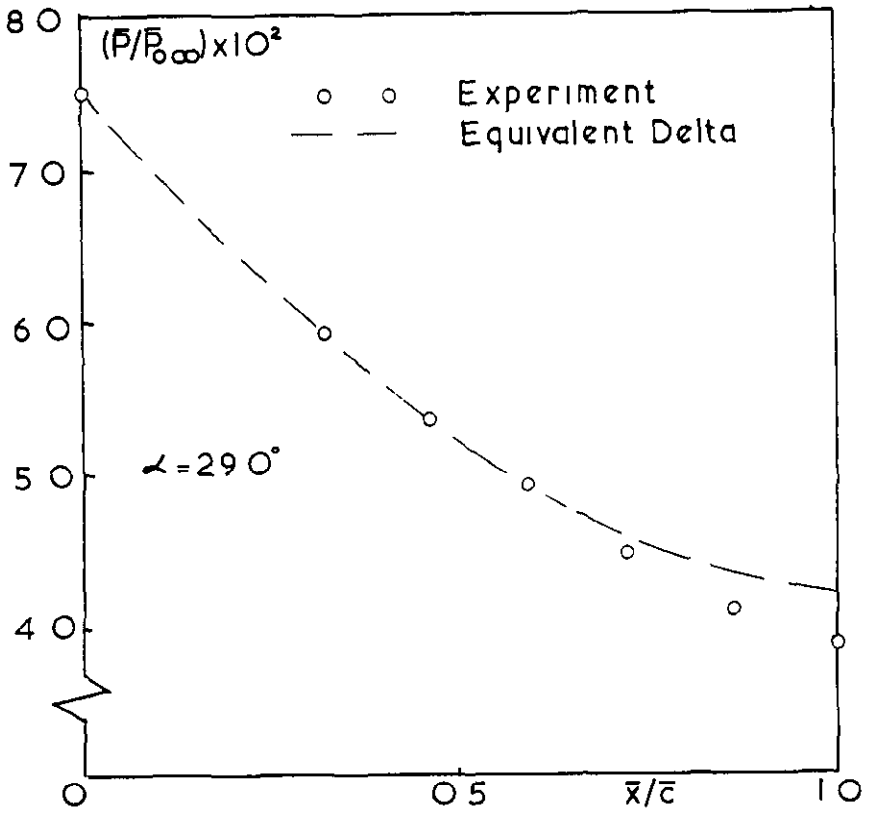

Figure 8 Centreline Pressure on Model 4 and the Equivalent Flat Delta

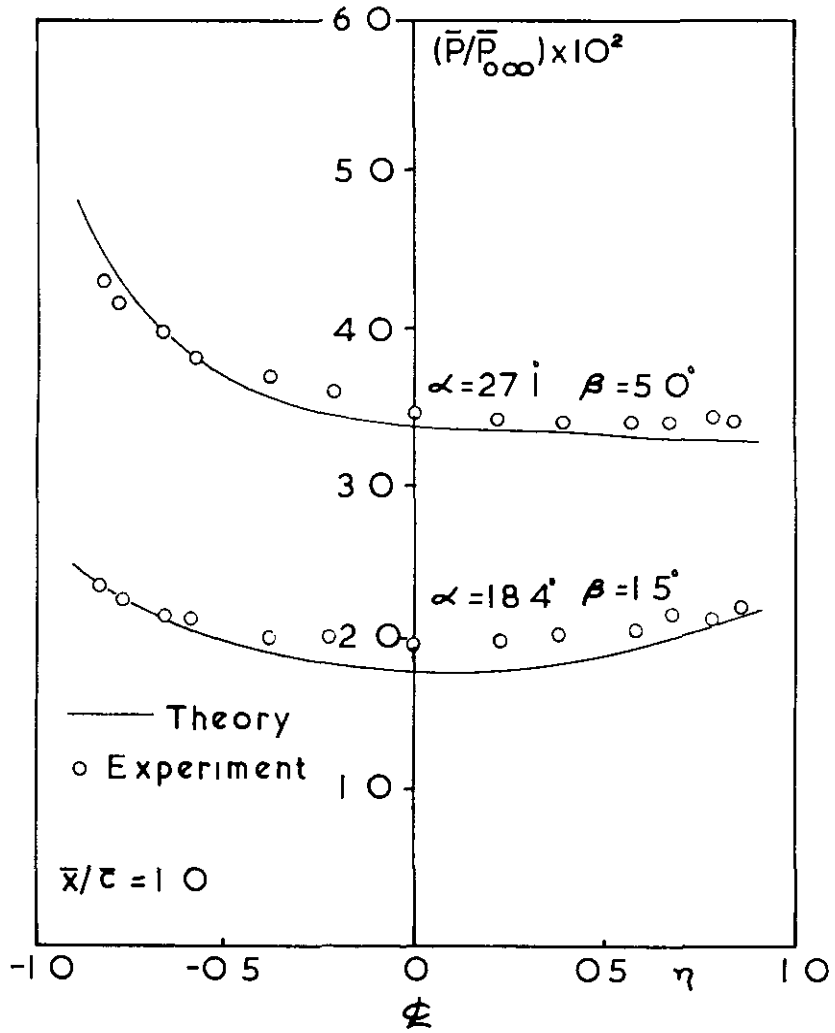

Figure 9 Comparison between Thin Shock Layer Theory and Experiment for Model 4

ARC CP No.1198
March 1971

Hillier, R.

PRESSURE DISTRIBUTIONS AT M_∞ = 3.51 AND AT HIGH INCIDENCES ON FOUR WINGS WITH DELTA PLANFORM

Results are presented for wind tunnel tests at M_∞ = 3.51 on four wings with pointed vertices and sharp leading edges. Two conical models were tested through a wide range of angles of incidence and yaw and the results clearly demonstrate the stabilising effect of dihedral. Two simple non-conical wings were also tested and it is shown, in this case, that the pressure on the compression surfaces may be approximately deduced from an 'equivalent' conical wing.

ARC CP No.1198
March 1971

Hillier, R.

PRESSURE DISTRIBUTIONS AT M_∞ = 3.51 AND AT HIGH INCIDENCES ON FOUR WINGS WITH DELTA PLANFORM

Results are presented for wind tunnel tests at M_∞ = 3.51 on four wings with pointed vertices and sharp leading edges. Two conical models were tested through a wide range of angles of incidence and yaw and the results clearly demonstrate the stabilising effect of dihedral. Two simple non-conical wings were also tested and it is shown, in this case, that the pressure on the compression surfaces may be approximately deduced from an 'equivalent' conical wing.

ARC CP No.1198
March 1971

Hillier, R.

PRESSURE DISTRIBUTIONS AT M_∞ = 3.51 AND AT HIGH INCIDENCES ON FOUR WINGS WITH DELTA PLANFORM

Results are presented for wind tunnel tests at M_∞ = 3.51 on four wings with pointed vertices and sharp leading edges. Two conical models were tested through a wide range of angles of incidence and yaw and the results clearly demonstrate the stabilising effect of dihedral. Two simple non-conical wings were also tested and it is shown, in this case, that the pressure on the compression surfaces may be approximately deduced from an 'equivalent' conical wing.

Produced and published by
HER MAJESTY'S STATIONERY OFFICE

To be purchased from
49 High Holborn, London WC1V 6HB
13a Castle Street Edinburgh EH2 3AR
109 St Mary Street, Cardiff CF1 1JW
Brazennose Street Manchester M60 8AS
50 Fairfax Street, Bristol BS1 3DE
258 Broad Street, Birmingham B1 2HE
80 Chichester Street, Belfast BT1 4JY
or through booksellers

Printed in England

C.P. No. 1198

SBN 11 470466 X